NOVEL MELT-PROCESSABLE NANOCOMPOSITES BASED ON ISOTACTIC POLYPROPYLENE AND CARBON NITRIDE: MORPHOLOGY, CRYSTALLIZATION AND DYNAMIC MECHANICAL PROPERTIES

Mohammed Naffakh,[1,*] Vicente López,[2] Félix Zamora,[2] and Marián A Gómez[1]

[1]Departamento de Física e Ingeniería de Polímeros, Instituto de Ciencia y Tecnología de Polímeros, CSIC, c/ Juan de la Cierva, 3, 28006, Madrid, Spain.

[2]Departamento de Química Inorgánica, Universidad Autónoma de Madrid, 28049 Madrid, Spain.

ABSTRACT: Light element-based materials like spherical carbon nitride (C_3N_4) particles were melt-mixed at different concentrations with isotactic polypropylene to produce new nanocomposites. The iPP/C_3N_4 nanocomposites were characterized with differential scanning calorimetry (DSC), time-resolved synchrotron X-ray scattering experiments and dynamic mechanical analysis (DMA). On the basis of the DSC experimental and theoretical analyses, the study of the dynamic crystallization kinetics provides a picture describing the physicochemical transformation of iPP molecules from the non-ordered state to the ordered state. The addition of C_3N_4 induces an increase of the crystallization rate and crystallinity of the polymer matrix, without variation of the crystalline structure of iPP. In the same way, the results of the nucleation activity confirmed the nucleating effect of C_3N_4 on the iPP crystallization. However, the addition of C_3N_4 causes an alteration of the effective energy barrier of the crystal growth process of iPP. The DMA studies revealed the reinforcing effect of the C_3N_4 on the mechanical performance of iPP with an increase in the storage modulus of around 32 %. Moreover, the heat deflection temperature of iPP increased considerably,

whereas the damping property was found to decrease because the C_3N_4 acted as barriers to the free movement of the iPP macromolecular chain.

Keywords Melt-processable nanocomposites, Isotactic polypropylene, Carbon nitride

*Corresponding author: Fax. +34 915644853
E-mail address: mnaffakh@ictp.csic.es (Mohammed Naffakh)

INTRODUCTION

Manufacturers fill polymers with synthetic or natural inorganic compounds in order to improve their properties, or simply to reduce cost. Conventional fillers are materials in the form of particles (e.g. calcium carbonate), fibers (e.g. glass fibers) or plate-shaped particles (e.g. mica). However, addition of conventional fillers sometimes imparts drawbacks to the resulting composites, such as weight increase, brittleness and opacity. Polymer/nanofiller composites, on the other hand, are a new class of composites consisting of inorganic and/or organic nanoparticles embedded in a polymer matrix (e.g. layered silicates, SiO_2, TiO_2, Al_2O_3, graphite, carbon nanotubes, hyperbranched polymers and dendrimers, etc.) (1-3). Consequently, polymer/nanofiller composites often exhibit advanced properties to conventional composites, such as strength, stiffness, thermal and oxidative stability, barrier properties, as well as flame retardant behaviour. These improved properties are generally attained at lower filler content in comparison with conventionally filled systems. Therefore, polymer/nanofiller composites are far lighter in weight than conventional composites, which make them quite competitive for specific applications (3).

Among the most versatile polymer matrices are polyolefins such as isotactic polypropylene (iPP). This thermoplastic is very widely used because of its high availability in the market, its wide range of properties, and its low cost. In spite of all these advantages, iPP has some deficiencies in mechanical properties for certain applications, like its low impact resistance at low temperatures, for example. To enhance its properties, one of the methods

used is to prepare composites by mixing the polymer with micro- and/or nanometric-sized reinforcements, which can act as nucleating agents (e.g. talc, glass fiber, sorbitol, carbon nanotubes, montmorillonite, POSS, nano-$CaCO_3$, nano-silica, IF-WS_2, etc.) (4-13). Nucleating agents are used routinely in polymer industry to shorten injection-moulding cycles and improve optical and mechanical properties (14-17). Non-isothermal processes are often useful and important for understanding the crystallization behaviour of iPP (18) due to their relationship to processing.

Light element-based materials such as graphite-like carbon nitride structures (g- C_3N_4 and g-CN) have been of particular interest due to their two-dimensional layered structures that are analogous to that of graphite. The layered structures may afford the ability to form tubular, belt-like and spherical structures analogous to that of layered graphite in forming carbon nanotubes, nanobelts and fullerenes. Progress has been made following the initial work by Liu and Cohen (19), in which covalently bonded carbon nitride (i.e. C_3N_4) was predicted to be as hard as diamond. Many efforts have been devoted to the synthesis of carbon nitrides by various chemical routes (20, 21). Such materials are important in high-performance engineering applications due to their unique properties, including low density, extreme hardness, wear resistance, chemical inertness, biocompatibility and special optical and electrical properties. Zimmerman et al first synthesized spherical C_3N_4 with the graphitic C_3N_4 layered structure, with diameters ranging from 20 microns to as few 30 nanometers, by reaction of $C_3N_3X_3$ (X: –Cl or –F) and Li_3N for its use in lubricants, catalyst supports, gas storage, and drug delivery (22). By a close related synthesis, we have recently been able to synthesize carbon nitride nanoparticles of C_3N_4 composition, by reaction between 1,3,5-trichlotriazine and sodium azide in toluene under mild solvothermal conditions. The bulk material thus obtained consists of spheres with diameters ranging from ~ 1 nm to 4 μm with a content of nanoparticles of 1-2 nm size, close to 20 % (23). In addition, new kind of graphite-

like carbon nitride nanobelt and nanotube have been synthesized using a simple solvothermal method at low temperature (24). Such materials have luminescent properties and may have potential uses as components of optical nanoscale devices.

In this work, regarding their properties, spherical carbon nitride fillers were incorporated into iPP matrix for the first time to investigate the effect of the filler on the thermal behaviour of the nanocomposite. The mechanical performance and structural behaviour were also characterized to examine the potential use of such materials. The iPP/C_3N_4 composites were prepared by melt-mixing as the most simple and effective method from both an economic and industrial perspective, because this process makes possible to fabricate high-performance nanocomposites at low cost, and facilitates commercial scale-up.

EXPERIMENTAL

Materials and processing

The polypropylene studied was an isotactic homopolymer provided by REPSOL-YPF (Spain) (25). The carbon nitride fillers were synthesized in the laboratory using a simple solvothermal method (23). Several concentrations of spherical C_3N_4 (0.1, 0.5, 1 and 2 wt. %) were introduced in the iPP matrix by melt-mixing using a micro-extruder (Thermo-Haake Minilab system) operated at 210 ºC and a rotor speed of 150 rpm for 10 min. Then, the samples were pressed as films of 0.5 mm thickness in a hot-press system using two heating/cooling plates.

Characterization techniques

The dispersion of C_3N_4 in the iPP matrix was characterized using a Philips XL30 ESEM scanning electron microscope (SEM) equipped with an energy dispersive X-ray (EDX) EDAX superUTW microanalytical system. The crystallization and melting behaviour of the nanocomposites were investigated by differential scanning calorimetry using a Mettler TA4000/DSC30. The experiments were carried out in a nitrogen atmosphere using approximately 12 mg of sample sealed in aluminium pans. Prior to the cooling and heating

scans, the samples were held at 210 ºC for 5 min to erase the thermal history of iPP. Then, the crystallization of the samples under non-isothermal conditions was carried out by cooling from 210 to 30 ºC. Four different crystallization experiments at cooling rates of at 2, 5, 10 and 15 ºC/min were performed. The dynamic-mechanical performance of the nanocomposites was studied using a dynamic mechanical analyzer (Mettler DMA861). The samples were cut in rectangular shapes with size of approx. 19.5×4×0.5 mm^3 and mounted in a large tension clamp. The measurements were performed in the tensile mode at various frequencies (0.1, 1 and 10Hz), in a temperature range between -100 and 100 °C with a heating rate of 2 °C/min. A dynamic force of 6 N oscillating at fixed frequency and amplitude of 30 μm was used. Simultaneous SAXS/WAXS experiments using synchrotron radiation were performed at the A2 beamline of the HASYLAB synchrotron facility (DESY, Hamburg). The experiments were performed with monochromatic X-rays of 0.15 nm wavelength using a germanium single crystal as the dispersing element. The scattering was detected with a linear Gabriel detector. The maximum of the Lorentz-corrected SAXS diffractograms was used to calculate the long period (L=1/smax) as a function of the temperature. Atomic force microscopy (AFM) images were obtained using Digital Instruments (Veeco) Nanoscope IVa (Tapping Mode) with Veeco RTESP7 Tips under ambient conditions. The C_3N_4 sample for AFM imaging was prepared using mica substrate containing 0.1wt. % nanoparticles mixed in acetone by sonication for 10 min.

RESULTS AND DISCUSSION

Morphological characterization of iPP/C_3N_4

The dispersion of C_3N_4 in the iPP matrix at the nanoscale is one of the most important features for reinforcing the polymer in the composite. SEM observation is used to directly and qualitatively visualize the state of dispersion of C_3N_4 in the iPP matrix due to the difficulty to prepare TEM samples including C_3N_4 rigid particles. Fig. 1 shows a typical image of the

fracture surface of the nanocomposite with 1wt. % of C_3N_4. The particle dimensions observed are in the range of 100 to 300 nm with a mean value of 190 nm and standard deviation of 35 nm. The C_3N_4 were uniformly dispersed at the nanoscale in the iPP matrix by the shear force exert during melt-blending without using modifiers or surfactants. On the other hand, the C_3N_4 sample for AFM imaging was prepared using mica substrate (Fig. 2). The height information from AFM images can be used as an exact particle diameter when spherical particles are investigated. AFM images show nanoparticles deposited on this surface with a maximum height of around 65 nm. Taking into account the AFM results and SEM resolution, we can conclude that the C_3N_4 dispersion in PP matrix takes place as small clusters of few particles up to the 2wt. % content considered here.

Dynamic crystallization behaviour and kinetics of iPP/C_3N_4

Crystallization of polymers releases a significant amount of heat that makes DSC a preferred method for measuring the overall crystallization kinetics. Fig. 3 shows the typical dynamic crystallization thermograms at various cooling rates for iPP/C_3N_4 nanocomposites. As the cooling rate increases, the crystallization exotherm broadens and shifts to lower temperatures for iPP and iPP/C_3N_4 composites, indicating that the lower the cooling rate, the earlier crystallization occurs. However, the most obvious result was the influence of C_3N_4 on the crystallization temperature of iPP for a particular cooling rate. The crystallization temperature of iPP increases with the incorporation of C_3N_4 at all cooling rates. This effect was clearly observed to be a function of composition, manifesting a significant increase of around 6 ºC of this parameter for the highest concentration of 2 wt. % of C_3N_4. In the same way, the crystallinity obtained during dynamic crystallization increases by a 9 % with the C_3N_4 content, from an average value of 53 % for iPP, to values of 55, 56, 57 and 58 % for the nanocomposites with 0.1, 0.5, 1 and 2 wt. %, respectively. For the estimation of the crystallinity of the samples, a value of 177 J/g for the melting enthalpy of 100 % crystalline

iPP was used (26). The increase in the crystallization temperature and crystallinity of iPP with increasing C_3N_4 content supports the nucleating effect of these kinds of particles in iPP crystallization. It is generally accepted that the addition of nanoparticles into the polymer matrix favors heterogeneous nucleation and thus is expected to make the molecular chains of polymer matrix easier to crystallize and increased the crystallization rate of composites in contrast to that of neat polymer (i.e. increase of peak crystallization temperature). Such a result has already been found with other nanocomposite systems, such as nylon-6/clay (27), PEN/Silica (28), nylon-6/SWCNT (29), iPP/SiO_2 (30), PEN/MWCNT (31) and iPP/IF-WS_2 (13).

Under the dynamic crystallization conditions previously described, iPP crystallized in the α, or monoclinic form. The WAXS diffractograms of iPP/C_3N_4 composites only present reflections associated to the crystalline planes characteristic of the monoclinic polymorph of iPP (13). No other crystalline forms of iPP were detected during cooling of the nanocomposites. In order to determine the influence of C_3N_4 on the lamellar structure of iPP, we have obtained the SAXS diagrams of the composites during the crystallization from the melt at 10 ºC.min^{-1}. The results obtained indicated that the addition of C_3N_4 caused no appreciable change in the long period (L) of iPP as the L values obtained at room temperature were almost the same for the nanocomposites (e.g. 15 nm for pure iPP and 16 nm for nanocomposite with 1wt. % of C_3N_4). From the results of the L data, the possible role of the C_3N_4 on the variation of thickness of the crystal lamellae of iPP can be investigated. As noted previously, L can be considered as the sum of the average thickness of the crystal lamellae and of the interlamellar amorphous regions. In addition, the parameter L and the crystallinity can also be used as a simple approximation to calculate the average thickness of the crystal lamellae of iPP. Therefore, the increase in crystallinity of the composites, observed from the

DSC data during the dynamic crystallization, could be connected to the increase of the size of the crystallites of iPP in the iPP/C_3N_4 composites.

In order to quantitatively describe the evolution of crystallinity during dynamic crystallization a number of models have been proposed in the literature. In this investigation, the Avrami, Ozawa and Lui analyses were tested.

Avrami analysis

In the Avrami model (32), the equivalent time-dependent degree of conversion is modeled as:

$$x(t) = 1 - \exp(-kt^n) \quad (1)$$

where *n* is the Avrami exponent that is associated with the crystallization mechanism (i.e. nucleation and growth) and *k* is the overall (macroscopic) rate constant. Plots of *ln(-ln(1-x)) vs. ln t* for iPP and its nanocomposite with 1wt. % of C_3N_4 are shown in Fig. 4. While the dependence shown is not linear over the entire range of crystalline transformation, there is a region over which the Avrami analysis appears to be valid. The values of Avrami exponent *n* for iPP, iPP/C_3N_4 (0.1wt. %), iPP/C_3N_4 (0.5wt. %), iPP/C_3N_4 (1wt. %) and iPP/C_3N_4 (2wt. %) range from 5.3 to 6.8, 4.7 to 6.8, 4.2 to 6.8, 5.7 to 6.8 and 4.5 to 6.8, respectively, which are higher than the average value of 3 obtained under isothermal crystallization conditions (33). The high values of *n* (more than 4) for these systems imply very complicated crystallization mechanisms. It is also note, that parameters such as *n* and *k* have an explicit physical meaning relating to isothermal crystallization, but in the dynamic crystallization their physical meaning does not have the same significance, due to the constant change in temperature, which influences both nucleation and crystal growth. Their use provides further insight into the kinetics of dynamic crystallization.

Ozawa analysis

Ozawa explained the effect of cooling rate on the dynamic crystallization by modifying the Avrami equation, assuming that the crystallization occurs at a constant cooling rate. According to Ozawa theory (34), the degree of conversion at temperature T (i.e. $x(T)$) can be calculated as:

$$1 - x(T) = \exp\left[-\frac{k'(T)}{\phi^m} \right] \quad (2)$$

where ϕ is the cooling rate, $k'(T)$ is a function related to the overall crystallization rate that indicates how fast crystallization proceeds, and m is the Ozawa exponent that depends on the dimension of crystal growth. By plotting $ln\ [ln(1-x(T))]$ *vs.* $ln\ \phi$ at a given temperature, a straight line should be obtained, if the Ozawa analysis is valid, and the kinetic parameters m and k' can be derived from the slope and the intercept, respectively. Some curvature in the plots of Fig. 5 was observed, indicating that the Ozawa is not consistent with temperature during dynamic crystallization, and this makes it difficult to estimate the cooling function, $k'(T)$ related to the overall crystallization rate. Therefore, we deduce that the Ozawa analysis does not effectively describe dynamic crystallization of iPP/C_3N_4 composites, probably because of the disregarded assumptions in the Ozawa's theory such as the ignorance of secondary crystallization, dependence of lamellar thickness on crystallization temperature and the constant value of cooling function over the entire crystallization process. Such a result has already been found with other polymer/nanofiller composites, such as PEN/silica (28), iPP/SiO_2 (30), PEN/ MWCNT (31) and PPS/IF-WS_2 (35).

Combined Ozawa-Avrami approach

From the above analysis, it is evident that the Avrami and Ozawa approaches do not describe the behaviour of iPP/C_3N_4 composites very satisfactorily. There have been attempts to modify and combine these two basic approaches to study the dynamic crystallization of polymers. In one such attempt, Lui at al. (36) derived new kinetic model to relate the degree of conversion

to the cooling rate and crystallization time. Therefore, their relationship for dynamic crystallization can be derived by combining the eqs. (1) and (2) as follows:

$$\ln \phi = \ln f(T) - \alpha \ln t \tag{3}$$

where $f(T) = [k'(T)/k]^{1/m}$, refers to the value of cooling rate chosen at unit crystallization time, when the system has a certain degree of crystallinity, α is the ratio of the Avrami exponents to Ozawa exponents (i.e. α=n/m). From eq. 3, the plots $ln\phi$ *vs.* $ln\ t$ at a certain degree of conversion are shown in Fig. 6, and these exhibit a good linear relationship, suggesting that this analysis may be more effective in describing the dynamic crystallization of iPP/C_3N_4 nanocomposites. The values of *f(T)* and α were determined from the slope and intercept of the plots and are listed in Table 1. It can be seen that the value of *f (T)* increased with increasing conversion (x), indicating that at unit crystallization time, a higher degree of conversion was obtained with a higher cooling rate. The value of α varies from 1.08 to 1.11 for the iPP, and from the 1.08 to 1.12 for iPP/C_3N_4 composites. However, the most important observation was the influence of C_3N_4 on the value of *f(T)* of iPP for a particular degree of conversion. The value of *f(T)* for neat iPP is higher than that for composites, which implies that the composites require a lower heating rate to approach an identical degree of crystalline transformation. This result suggests that the presence of C_3N_4 acts as nucleating sites for the dynamic crystallization process of iPP.

Nucleation ability

In order to analyze the nucleation ability of C_3N_4 in iPP composites two models have been proposed in the literature. In this investigation, the Dobreva-Gutzow and Fillon models were tested. Dobreva and Gutzow (37, 38) developed a simple method for calculating the nucleation activity of foreign substrates in polymer melt. Nucleation activity (φ) is a factor by which the three-dimensional nucleation process decreases with the addition of a foreign substrate. If the foreign substrate is extremely active, φ approaches 0, while for inert particles,

φ approaches 1. For homogeneous nucleation from a melt near the melting temperature, the cooling rates can be written as:

$$\ln \phi = A - \frac{B}{\Delta T_p^2} \tag{4}$$

while for the heterogeneous case,

$$\ln \phi = A - \frac{B^*}{\Delta T_p^2} \tag{5}$$

$$\varphi = \frac{B^*}{B} \tag{6}$$

where ϕ is the cooling rate, A is a constant, and ΔT_p is the degree of supercooling, i.e. $\Delta T_p = T_m - T_c$, and T_c is the temperature corresponding to the peak temperature of the DSC crystallization curves. B is a parameter that can be calculated from the following equation:

$$B = \frac{\omega \sigma^3 V_m^2}{3 n k_B T_m^0 \Delta S_m^2} \tag{7}$$

where ω is a geometrical factor; σ is the specific energy, V_m is the molar volume of the crystallizing substance, n is the Avrami exponent, ΔS_m is the entropy of melting, k_B is the Boltzman constant and T_m^0 is the infinite crystal melting temperature. The values of B and B^* can be calculated for iPP and the composites, respectively, from the slopes of the linear plots of eqs. 4 and 5, considering a value of 196 ºC for the thermodynamic equilibrium melting temperature of iPP (33). As shown in Fig. 7, the addition of C_3N_4 cause a reduction of φ which reaches a value of 0.68 for a concentration of 2 wt. % of C_3N_4, indicating that C_3N_4 can act as a nucleating agent in the iPP matrix.

The nucleation efficiency can also be determined from the variation observed in the crystallization temperature of the iPP matrix in the composites with respect to that found in the same matrix by an auto nucleation process at the same cooling rate. In this case, the concentration and distribution of crystalline nuclei and the nucleus-matrix interaction can be considered ideal, and the nucleation efficiency should be at its maximum (39, 40). Given that

the two extremes in the efficiency scale are the non-nucleated matrix and the auto nucleated matrix, the nucleation efficiency (*NE*) can be expressed as:

$$NE = \frac{T_c - T_{c1}}{T_{c2\max} - T_{c1}} \times 100 \quad (8)$$

where T_{c1} and T_{c2max} are the crystallization temperatures of the non-nucleated and best self-nucleated PP, respectively and T_c is the crystallization temperature obtained in the presence of the C_3N_4 nanoparticles. A value of 140 ºC was used for T_{c2max} obtained from self-nucleation experiments reported by Marco et al. (25) for the polypropylene used in our study, whereas the lower temperature T_{c1} is 113.4 ºC calculated from the data of Fig. 3 for a cooling rate of 10ºC/min (i.e. a difference of 26.6 ºC defines the efficiency scale). Under these considerations, values for *NE* from 3 % to 20 % were obtained for C_3N_4 concentrations between 0.1 % and 2 %, for a cooling rate of 10 ºC/min. These moderate values were reported in the literature for other iPP nanocomposites modified using silica, MMT and $CaCO_3$ nanoparticles (9, 11, 12). In the case of MMT for filler contents between 5% and 10%, a nucleating efficiency above 20% was reached (27% and 35% respectively). Nucleation efficiency values above 50% are only obtained by using advanced inorganic fullerene-like WS_2 (13) and selective nucleating agents based, for example, on sorbitols (7, 40) and sodium salt derivatives (25) used as specific nucleating additives at concentrations up to 1wt.%. In Fig. 7, the evolution of both the nucleating activity and the nucleating efficiency are compared as a function of the concentration for the iPP/C_3N_4 composites analyzed in this investigation.

Effective energy barrier

Apart from the nucleation ability it is interesting also to evaluate the effective energy barrier (ΔE) for the dynamic crystallization process in order to estimate the growth ability of the chain segments. The higher ΔE, the more difficult is the transport of macromolecular segments to the growing surface. It is well-known that the crystallization from the melt-state

involves simultaneous nucleation and growth during the initial stage, while from the region closer to the crystallization peak the process is mainly dominated by growth, i.e. nucleation if at all exists becomes negligible from the region nearer to the crystallization peak and the process becomes isokinetic. Several procedures have been proposed in the literature for the calculation of ΔE (41, 42). Among them the Kissinger method has been widely used in evaluating the overall effective energy barrier (43):

$$\ln(\frac{\phi}{T_p^2}) = Cons\tan t - \frac{\Delta E}{RT_p} \quad (9)$$

where R is the universal gas constant, the rest of the parameters being described previously. From the slopes of the linear plots of eq. 9, the values of ΔE can be calculated for iPP and the composites, respectively (Table 1). The addition of C_3N_4 nanoparticles caused a decrease of ΔE which made the molecular chains of iPP easier to crystallize, and increased the crystallization rates due to the nucleation effect of the C_3N_4. However, the further addition of C_3N_4 (i.e. from 0.5 to 1 and 2wt. %) may lead to a positive effect on the nucleation process but a negative impact on the transport of iPP segments to the growing surface (i.e. increase of ΔE). As a consequence, the increase of C_3N_4 concentration alters the competing factors affecting the crystallization behaviour of iPP (i.e. opposing effects of nucleation and crystal growth rates), which indicates that the crystallization becomes strongly controlled by the transport process.

Dynamic mechanical behaviour iPP/C_3N_4

DMA is often used to study relaxations in polymers. An analysis of storage modulus and *tan* δ curves is very useful in ascertaining the performance of a sample under stress and temperature. A clear understanding of the storage modulus–temperature curve obtained during a dynamic mechanical test provides valuable insight into the stiffness of a material as a function of temperature. Fig. 12 shows the dynamic mechanical data of iPP and iPP/C_3N_4

nanocomposites. When the C_3N_4 nanoparticles are incorporated the stiffness of composites increases, resulting in high storage modulus of iPP matrix over the entire temperature range. Measurements of storage modulus at room temperature revealed a percolative behaviour with an extremely low percolation threshold. By adding only 0.1wt. % of C_3N_4, the storage modulus of iPP increase by 32 %. Also the addition of C_3N_4 nanoparticles allows greater heat resistance of iPP, which consequently increases the heat deflection temperature of iPP. To evaluate the heat resistance of the nanocomposites, we define the temperature at 1300 MPa (i.e. storage modulus of iPP at 25 ºC) as T_{1300} (44). From Fig. 12.a, it is observed that T_{1300} = 41 °C for the nanocomposite containing 0.1 wt. % of C_3N_4. These results imply that the heat deflection temperature of iPP can be significantly improved by incorporation of C_3N_4.

Damping or loss factor ($tan\delta$) is an important parameter related to the study of dynamic behaviour of nanocomposite structures. $tan\ \delta$ relates to the impact resistance of the material (45). The variation of $tan\ \delta$ of the iPP/C_3N_4 nanocomposites as a function of temperature is shown in Fig. 12. a. It can be seen that the value of $tan\ \delta_{max}$ of iPP decreases with the addition of C_3N_4. Incorporation of C_3N_4 acted as barriers to the mobility of iPP chains leading to lower flexibility, lower degrees of molecular motion and hence lower damping characteristics. On the other hand, it is well known that the glass transition temperature (T_g) of a polymer matrix tends to increase with the addition of nanoparticles. In our case, all samples were prepared following the same procedure, but because of the rapid crystallization of iPP, the samples showed higher crystallinity values of iPP in the nanocomposites (see the DSC results). Thus, it is expected that the T_g of iPP would show higher temperature values in the nanocomposites. However, Fig. 12.a indicates that the addition of C_3N_4 caused no measurable change in the T_g as indicated by the fact that the peak near 4 ºC did not change position. Thus, the anticipated effect of C_3N_4 nanoparticles on the T_g of iPP was masked. A more detailed study concerning the addition of a third component (e.g. toughening agent like triblock copolymer SEBS) is in

progress. The main objective is to improve the dispersion and to optimize the balance between impact strength and stiffness of PP nanocomposites based on C_3N_4 rigid particles.

CONCLUSIONS

The preparation and properties of isotactic polypropylene (iPP)/carbon nitride (C_3N_4) nanocomposites are reported. The resulting nanocomposites showed a good dispersion of C_3N_4 in the polymer matrix without using modifiers or surfactants. The crystallization temperature for the iPP/C_3N_4 nanocomposites decreased with increasing cooling rate for a given C_3N_4 content and increased with C_3N_4 content for a given cooling rate. The introduction of C_3N_4 changed the crystallization kinetics as evidenced by the experimental and theoretical analyses, whilst maintaining the monoclinic crystalline structure of iPP. Combined Ozawa-Avrami approach was found to be effective in describing the crystallization behaviour of iPP/C_3N_4 nanocomposites. All rate parameters (e.g. *f(T)*) suggested that the addition of C_3N_4 caused an increase of the crystallization rate of iPP due to the nucleating effect of C_3N_4. This nucleation phenomenon is manifested by a moderate variation of the nucleation activity parameters (e.g. $\leq$20%). However, the incorporation of C_3N_4 causes an alteration of the apparent effective energy barrier, which induces a change from promotion to retardation of the crystal growth process of iPP. Finally, dynamic mechanical measurements revealed a percolative behaviour with an extremely low percolation threshold. The storage modulus of iPP increase considerably with the addition of C_3N_4 at the expense of the reduction in the damping property due to the decrease of the free movement of the iPP macromolecular chains.

ACKNOWLEDGEMENTS

Dr. M. Naffakh would like to express his sincere thanks to the Consejo Superior de Investigaciones Cientificas (CSIC) for postdoctoral contract (I3PDR-6-02), financed by the European Social Fund, the European Commission for the X-ray synchrotron experiments

performed at the Soft Condensed Matter A2 beamline at HASYLAB (DESY-Hamburg, I-20090038 EC) and the Spanish MICINN for national projects (NAN2004-09183-C10-02/06, MAT2006-13167-C01 and MAT2007-66476-C02-02).

REFERENCES

[1] Giannelis, E. P. (1996). *Adv. Mater.*; 8: 29-35.

[2] Rozenberg, B. A., and Tenne, R. (2008). *Prog. Polym. Sci.*; 33: 40-112.

[3] Pavlidou, S., and Papaspyrides, C. D. (2008). *Prog. Polym. Sci.*; 33: 1119-98.

[4] Velasco, J. I., De Saja, J., and Martínez, A. B. (1996). *J. Appl. Polym. Sci.*; 61: 125-32.

[5] Karger-Kocsis, J. (1995) Polypropylene: Structure, blends and composite vol 3 Composites; Chapman & Hall, London.

[6] Marco. C., Gómez, M. A., Ellis, G. and Arribas, J. M. (2002). *J. Therm. Anal. Cal.*; 68: 61-74.

[7] Marco, C., Gómez, M. A., Ellis, G. and Arribas, J. M. (2002). *J. Appl. Polym. Sci.*; 84: 2440-2450.

[8] Assouline, E., Lustiger, A., Barber, A. H., Cooper, C. A., Klein, E., Wachtel, E., and Wagner, H, D. (2003). *J. Polym. Sci. Part B: Polym. Phys.*; 41: 520-27.

[9] Xu, W., Ge, M., and He, P. (2002). *J. Polym. Sci. Part B Polym. Phys.*; 40: 408-414.

[10] Chen, J. H., and Chiou, Y. D. (2006). *J. Polym. Sci. Part B: Polym. Phys.*, 44: 2122-34.

[11] Lin, Z., Huang, Z., Zhang, Y., Mai, K., and Zeng, H. (2004). *J. Appl. Polym. Sci.*; 91: 2443-53.

[12] Jain, S., Goossens, H., Van Duin, M., and Lemstra, P. (2005). *Polymer*; 46: 8805-18.

[13] Naffakh, M., Martín, Z., Fanegas, N., Marco, C., Gómez, M. A., and Jiménez, I. (2007). *J. Polym. Sci. Part. B: Polym. Phys.*; 45: 2309-21.

[14] Tordjeman, Ph., Robert, C., Marin, G., and Gerard, P. (2001). *Eur. Phys. J. E*; 4: 459-65.

[15] Chan, C. M., Wu J., Li, J. X., and Cheung, Y. K. (2002). *Polymer*; 43: 2981-92.

[16] Thierry, A., Straupe, C., Wittmann, J. C., and Lotz, B. (2006). *Macromol. Symp.*; 241: 103-10.

[17] Libster, D., Aserin, A., and Garti, N. (2007). *Polym. Adv. Technol.*; 18: 685-95.

[18] Varga, J. (1992). *J. Mater. Sci.*; 27: 2557-79.

[19] Liu, A. Y., and Cohen, M. L. (1989). Science; 245: 841-42.

[20] Wang, E. G. (1997). *Prog. Mater. Sci.;* 41: 241-98.

[21] Goglio, G., Foy, D., and Demazeau, G. (2008). *Mater. Sci. Eng.* R; 58: 195-27.

[22] Zimmerman, J. L., Williams, R., Khabashesku, V. N., and Margrave, J. L. (2001). *Nano Lett.*; 1: 731-34.

[23] López, V., Román-Pérez, G., Arregui, A., Mateo-Marti, E., Bañares, L., Martín-Gago, J. A., Soler, J. M., Gómez-Herrero, J., and Zamora, F. (2009). *ACS Nano*; 3: 3352-57.

[24] Li, J., Cao, C., Zhu, H. (2007). *Nanotechnology*; 18 art. no.115605.

[25] Marco, C., Gómez, M. A., Ellis, G., and Arribas, J. M. (2002). *J. Appl. Polym. Sci.*; 84: 1669-79.

[26] Li, J. X., Cheung, W. L., and Demin, J. (1999). *Polymer*; 40: 1219-22.

[27] Devaux, E., Bourbigot, S., and El Achari, A. (2002). *J. Appl. Polym. Sci.*; 86: 2416-23.

[28] Kim, S. H., Ahn, S. H. and Hirai, T. (2003). *Polymer*; 44: 5625-34.

[29] Naffakh, M., Marco, C., Gómez, M. A., Ellis, G., Maser, W. K., Benito, A. and Martínez, M. T. (2009). *J. Nanosci. Nanotechnol*; 9 (10): 6120-26.

[30] Papageorgiou, G. Z., Achilias, D. S., Bikiaris, D. N., and Karayannidis G. P. (2005). *Thermochim Acta*; 427: 117-28.

[31] Kim, J. Y., Park, H. S., and Kim, S. H. (2006). *Polymer*; 47:1379-89.

[32] Avrami, M. (1939). *J. Chem. Phys.*; 7: 1103-112; (1940). *J. Chem. Phys.*; 8: 212-24; (1941). *J. Chem. Phys.*; 9: 177-84.

[33] Naffakh. M., Martín, Z., Marco, C., Gómez, M. A. and Jiménez, I. (2008). *Thermochim. Acta*; 472: 11-16.

[34] Ozawa, T. (1971). *Polymer*; 12: 150-58.

[35] Naffakh, M., Marco, C., Gómez, M. A. and Jiménez, I. (2009). *J. Phys. Chem. B*; 113: 7107-15.

[36] Liu, T., Mo, Z., Wang, S., and Zhang, H. (1997). *Polym. Eng. Sci.*; 37: 568-75.

[37] Dobreva, A., and Gutzow, I. (1993). I. Theory *J. Non-Cryst. Solids*; 162: 1-12.

[38] Dobreva, A., and Gutzow, I. (1993). *J. Non-Cryst. Solids*; 162: 13-25.

[39] Fillon, B., Lotz, B., Thierry, A., and Wittmann, J. C. (1993). *J. Polym. Sci. Polym. Phys.*; 31: 1395-05.

[40] Fillon, B., Thierry,A.,Lotz, B., and Wittmann, J. C.(1994). *J. Therm. Anal. Cal.*;42:721-31.

[41] Sbirrazzuoli, N., Girault, Y., and Elégant, L. (1997). *Thermochim. Acta*; 293; 25-37.

[42] Di Lorenzo, M. L., and Silvestre, C. (1999). *Prog. Polym. Sci.*; 24: 917-50.

[43] Kissinger, H. E. (1956). *J. Res. Natl. Bur. Stand.*; 57: 217-21.

[44] Huang, Li., Yuan, Q., Jiang, W., An, L., Jiang, S., and Li, R. K. Y. (2004). *J. Appl. Polym. Sci.*; 94: 1885-90.

[45] Sepe, M. P. (1992). *Adv. Mater. Process.*; 4: 32-35.

TABLE 1. Values of α and *f(T) versus* conversion (x) based on Liu model for iPP/C_3N_4 nanocomposites.

C_3N_4 content (%)	**x (%)**	**α**	***f(T)***	***ΔE* (kJ/mol)[a]**
0	10	1.08	120.03	-316.1
	30	1.08	123.33	
	50	1.08	126.71	
	70	1.10	133.94	
	90	1.11	148.96	
0.1	10	1.08	120.21	-332.5
	30	1.08	123.67	
	50	1.09	127.05	
	70	1.09	131.80	
	90	1.11	143.75	
0.5	10	1.08	117.85	-369.6
	30	1.08	120.28	
	50	1.09	123.77	
	70	1.09	128.61	
	90	1.11	139.31	
1	10	1.09	118.96	-308.0
	30	1.09	121.57	
	50	1.09	125.10	
	70	1.10	131.24	
	90	1.12	142.28	
2	10	1.09	114.95	-285.7
	30	1.09	118.88	
	50	1.10	122.67	
	70	1.11	129.10	
	90	1.12	140.55	

[a] Effective energy barrier calculated using Kissinger´s equation.

Figure captions

FIGURE 1. Bottom panel: SEM micrographs of iPP/C_3N_4 (1wt. %) composite. Top panel: Size distribution of the C_3N_4 nanoparticles.

FIGURE 2. AFM images of C_3N_4 nanoparticles**.**

FIGURE 3. DSC thermograms of dynamic crystallization of (a) iPP and (b) iPP/C_3N_4 (2wt. %) obtained at various cooling rates; inset is the plot of crystallization temperature (T_c) *versus* cooling rate.

FIGURE 4. Avrami plots of the crystallization of (a) iPP and (b) iPP/C_3N_4 (1wt. %).

FIGURE 5. Ozawa plots of the crystallization of (a) iPP and (b) iPP/C_3N_4 (1wt. %).

FIGURE 6. Liu plots of the crystallization of (a) iPP and (b) iPP/C_3N_4 (1wt. %).

FIGURE 7. Variation of φ and *NE* of C_3N_4 with concentration for iPP/C_3N_4 composites.

FIGURE 8. Dynamic mechanical analysis of iPP/C_3N_4 nanocomposites obtained at a frequency of 1 Hz: (a) storage modulus and loss factor *versus* temperature and (b) value of storage modulus obtained at room temperature versus C_3N_4 concentrations.

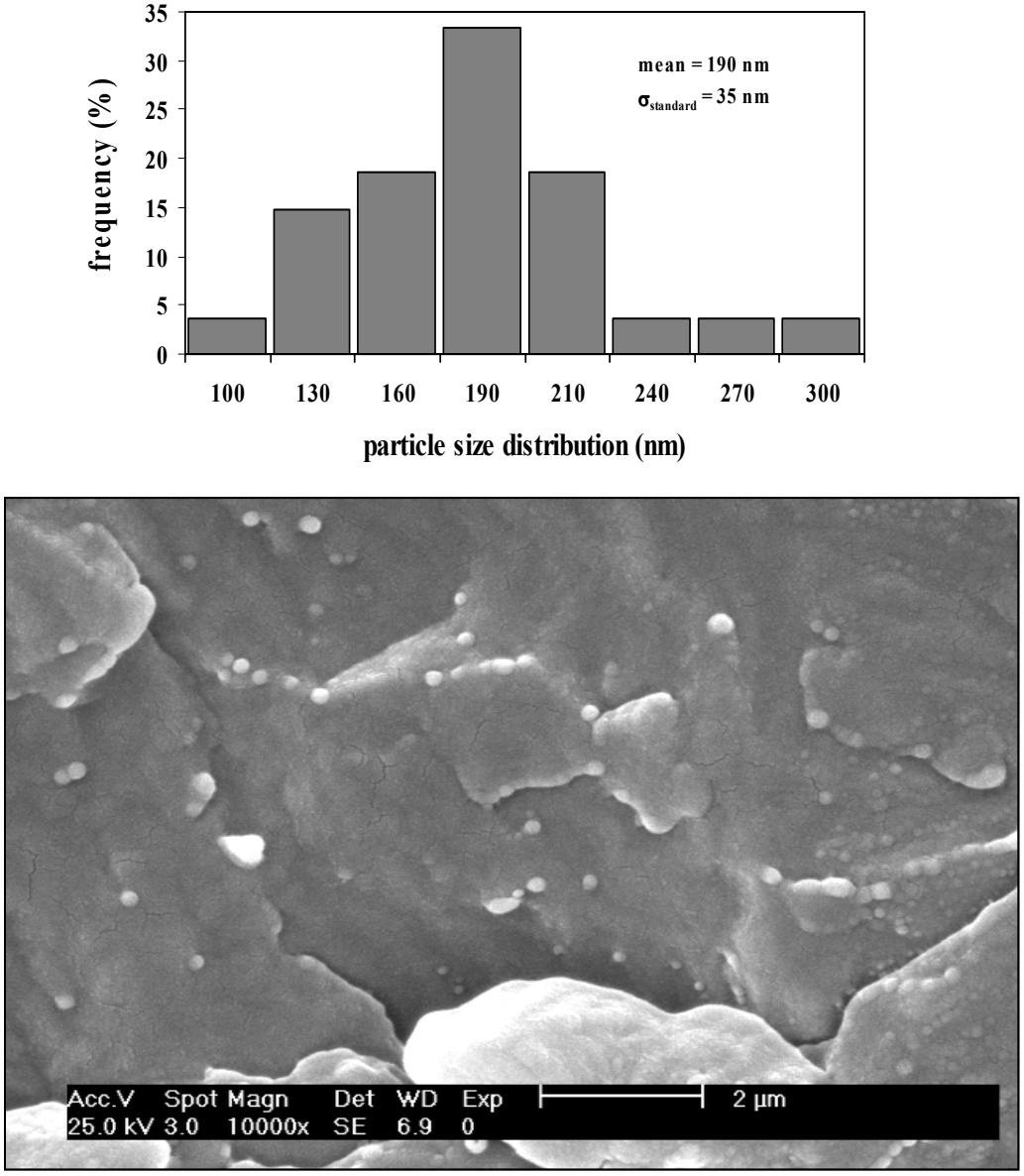
35
30
25
20
15
10
5
0
frequency (%)
mean = 190 nm
σstandard = 35 nm
100
130
160
190
210
240
270
300
particle size distribution (nm)
Acc.V Spot Magn Det WD Exp
25.0 kV 3.0 10000x SE 6.9 0
2 µm

FIGURE 1.

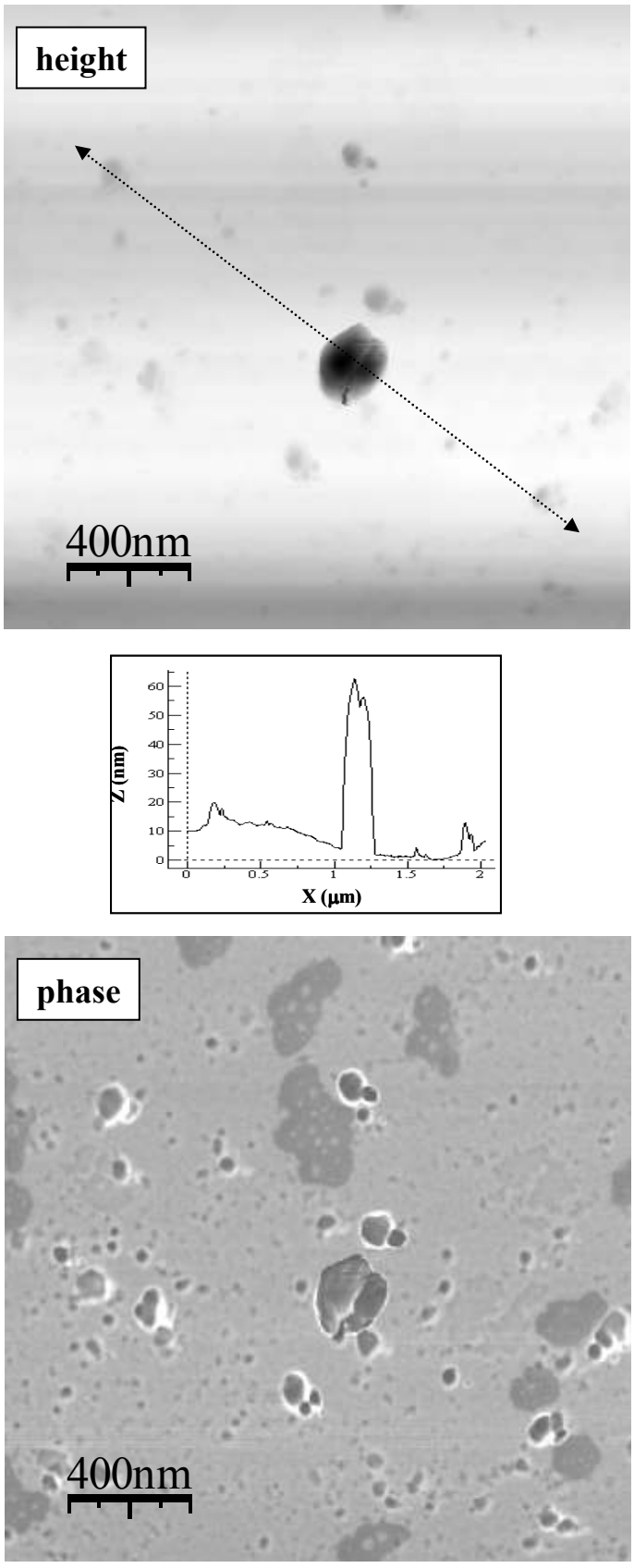

FIGURE 2.

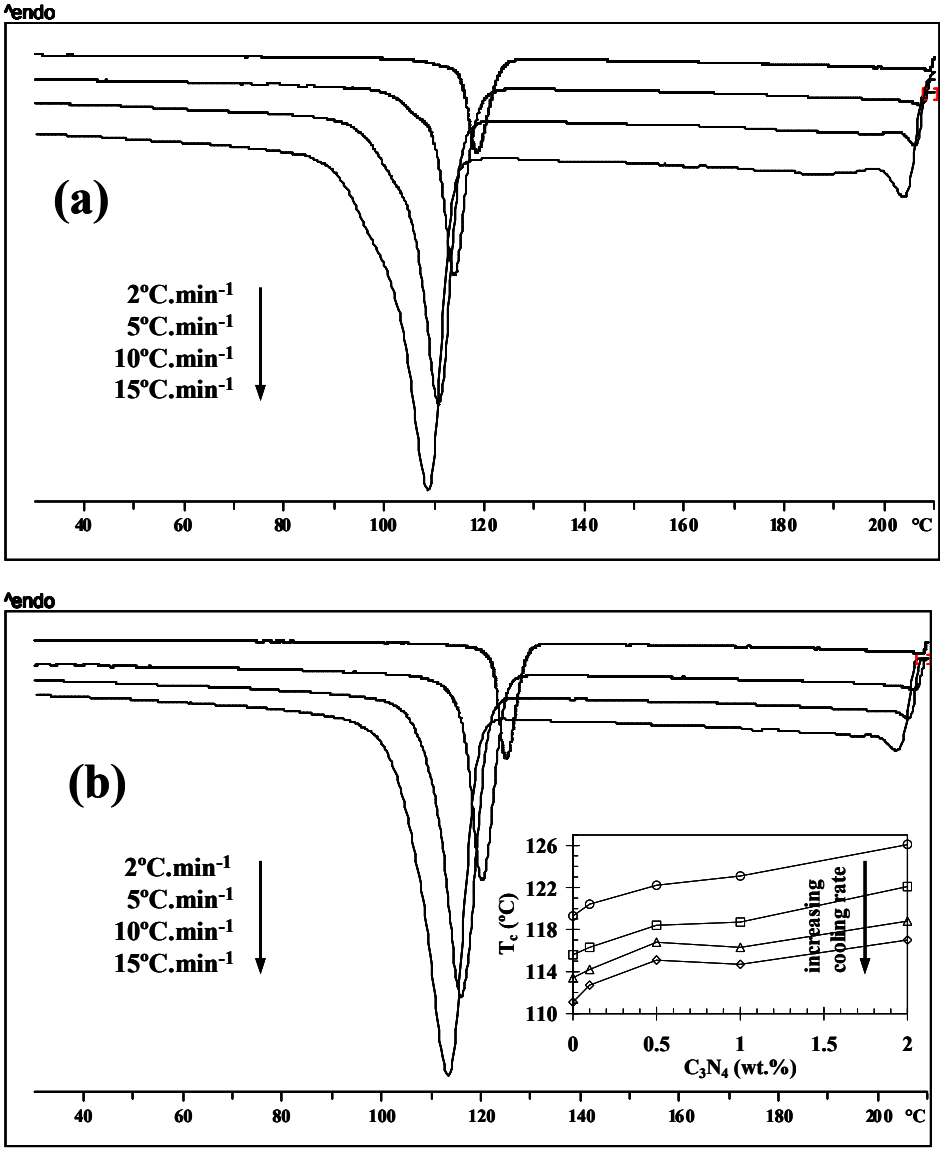
^endo
(a)
2ºC.min-1
5ºC.min-1
10ºC.min-1
15ºC.min-1
40
60
80
100
120
140
160
180
200
°C
^endo
(b)
2ºC.min-1
5ºC.min-1
10ºC.min-1
15ºC.min-1
Tc (°C)
126
122
118
114
110
0
0.5
1
1.5
2
C3N4 (wt.%)
increasing cooling rate
40
60
80
100
120
140
160
180
200
°C

FIGURE 3.

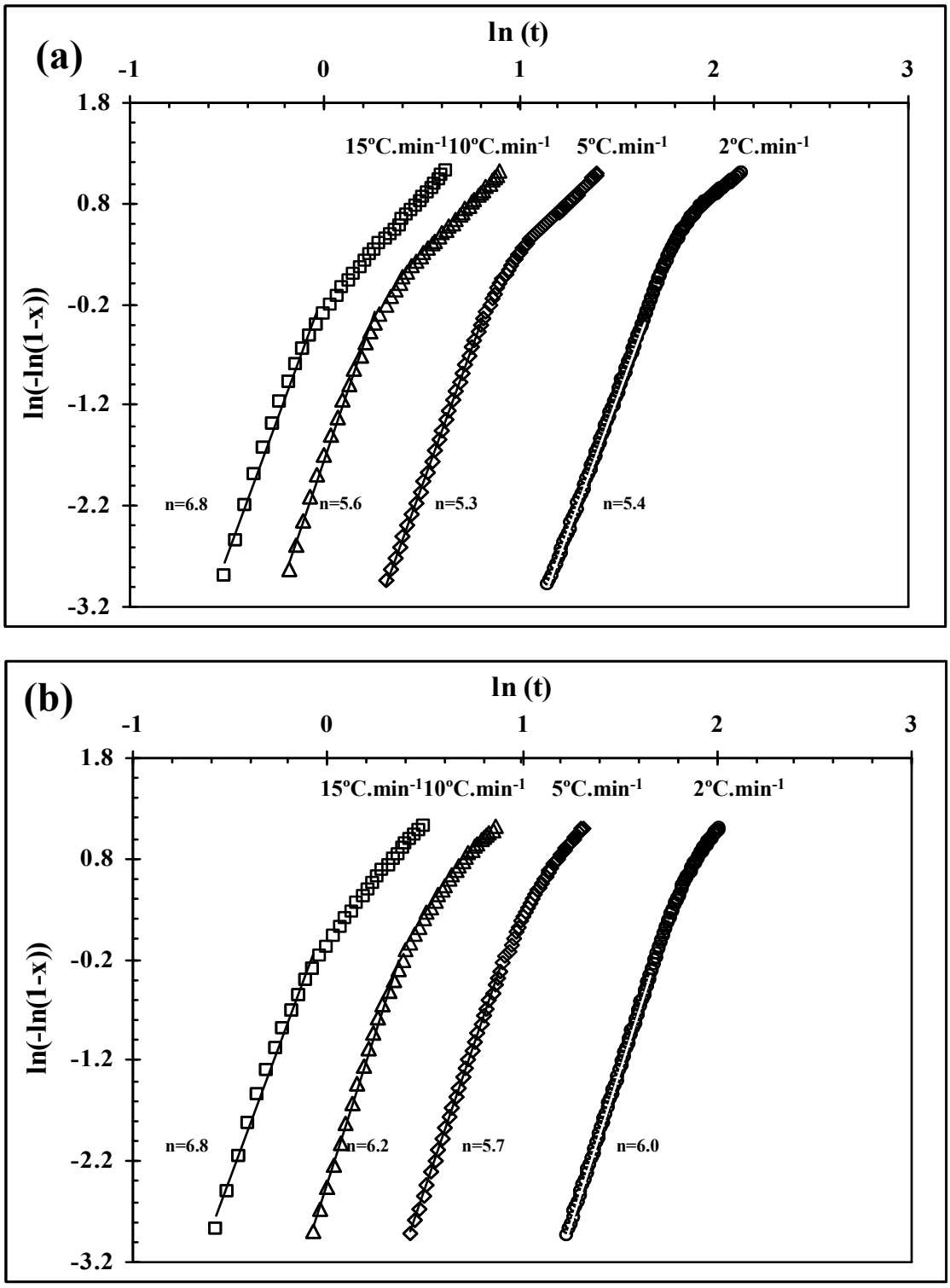
(a)
ln (t)
-1
0
1
2
3
1.8
0.8
-0.2
-1.2
-2.2
-3.2
ln(-ln(1-x))
15ºC.min-1
10ºC.min-1
5ºC.min-1
2ºC.min-1
n=6.8
n=5.6
n=5.3
n=5.4
(b)
ln (t)
-1
0
1
2
3
1.8
0.8
-0.2
-1.2
-2.2
-3.2
ln(-ln(1-x))
15ºC.min-1
10ºC.min-1
5ºC.min-1
2ºC.min-1
n=6.8
n=6.2
n=5.7
n=6.0

FIGURE 4.

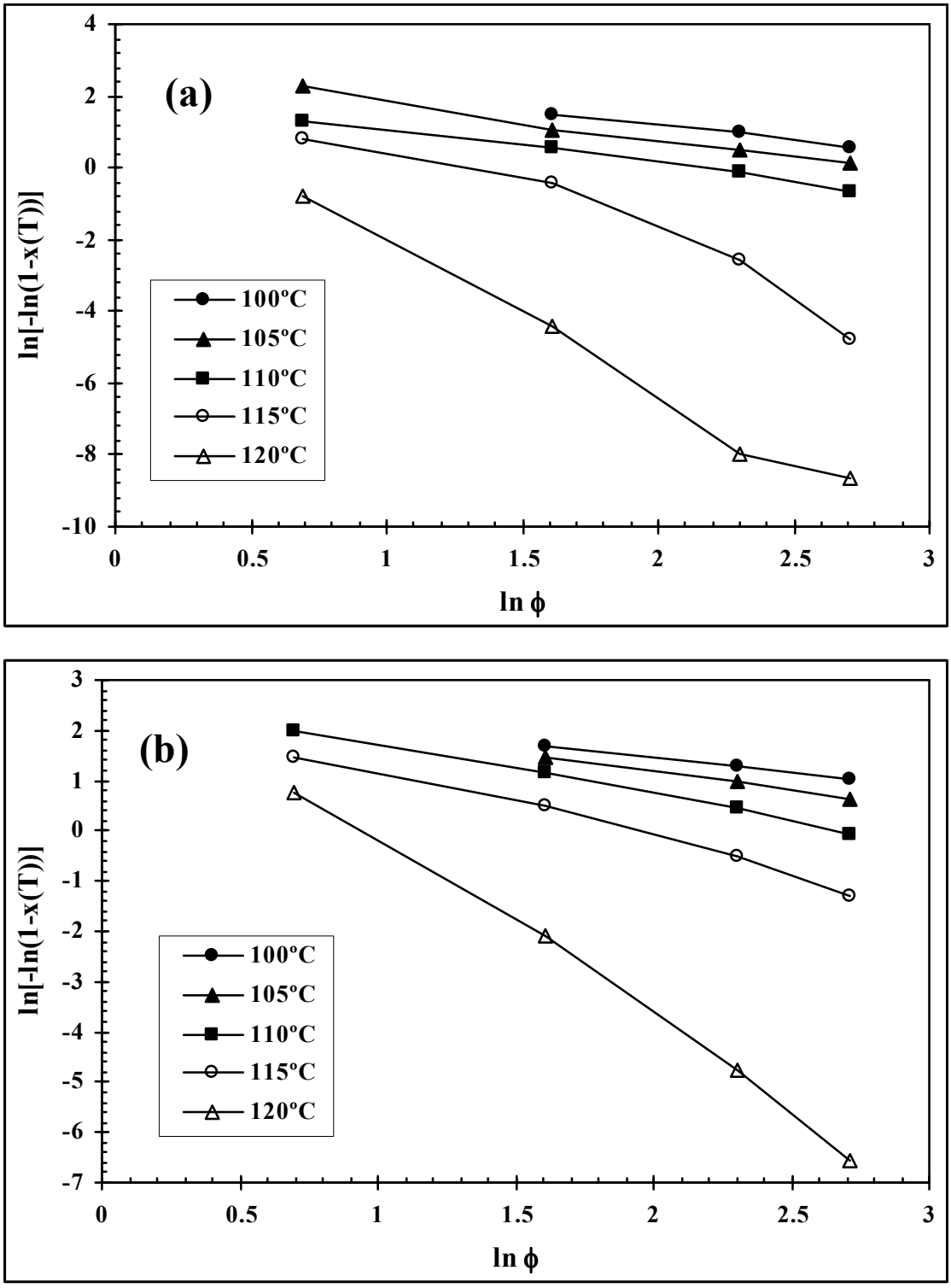
(a)
ln[-ln(1-x(T))]
ln ϕ
100°C
105°C
110°C
115°C
120°C
(b)
ln[-ln(1-x(T))]
ln ϕ
100°C
105°C
110°C
115°C
120°C

FIGURE 5.

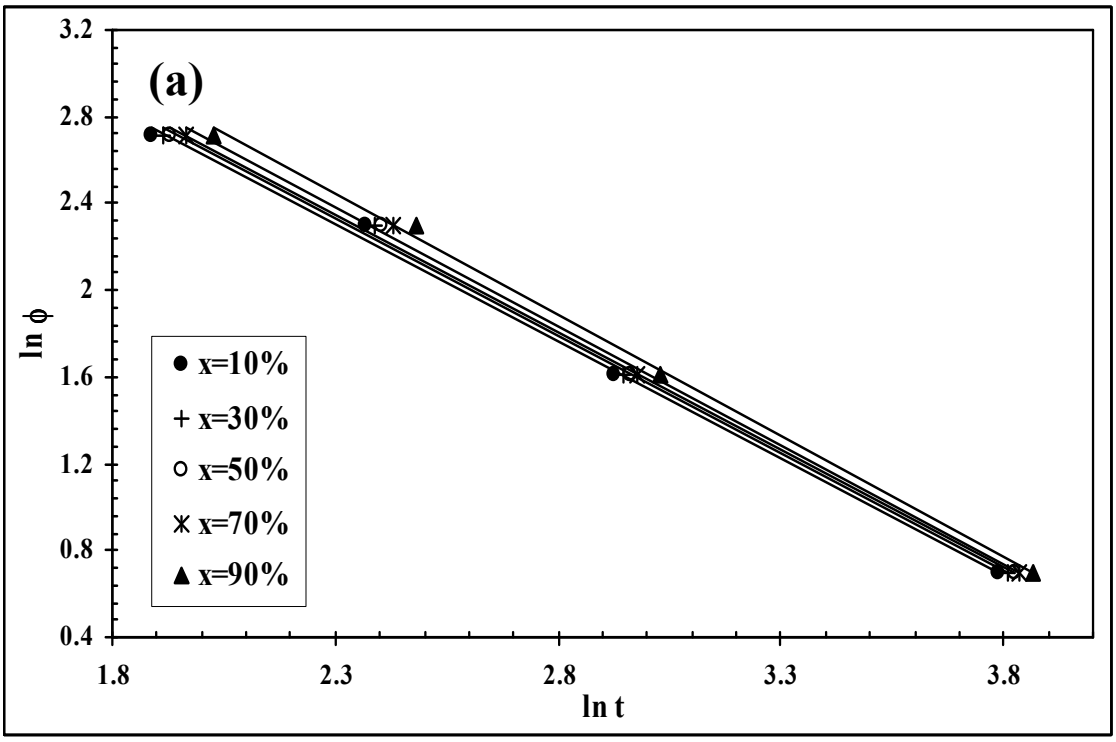
(a)
3.2
2.8
2.4
2
1.6
1.2
0.8
0.4
ln ϕ
1.8
2.3
2.8
3.3
3.8
ln t
x=10%
x=30%
x=50%
x=70%
x=90%

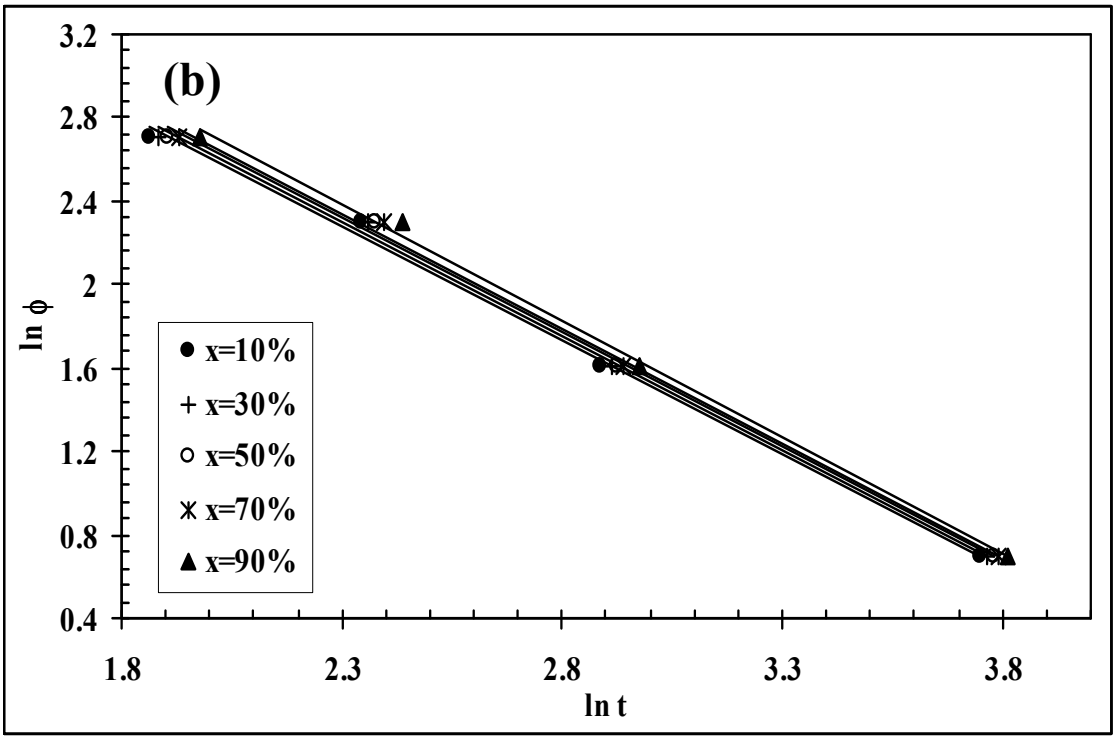
(b)
3.2
2.8
2.4
2
1.6
1.2
0.8
0.4
ln ϕ
1.8
2.3
2.8
3.3
3.8
ln t
x=10%
x=30%
x=50%
x=70%
x=90%

FIGURE 6.

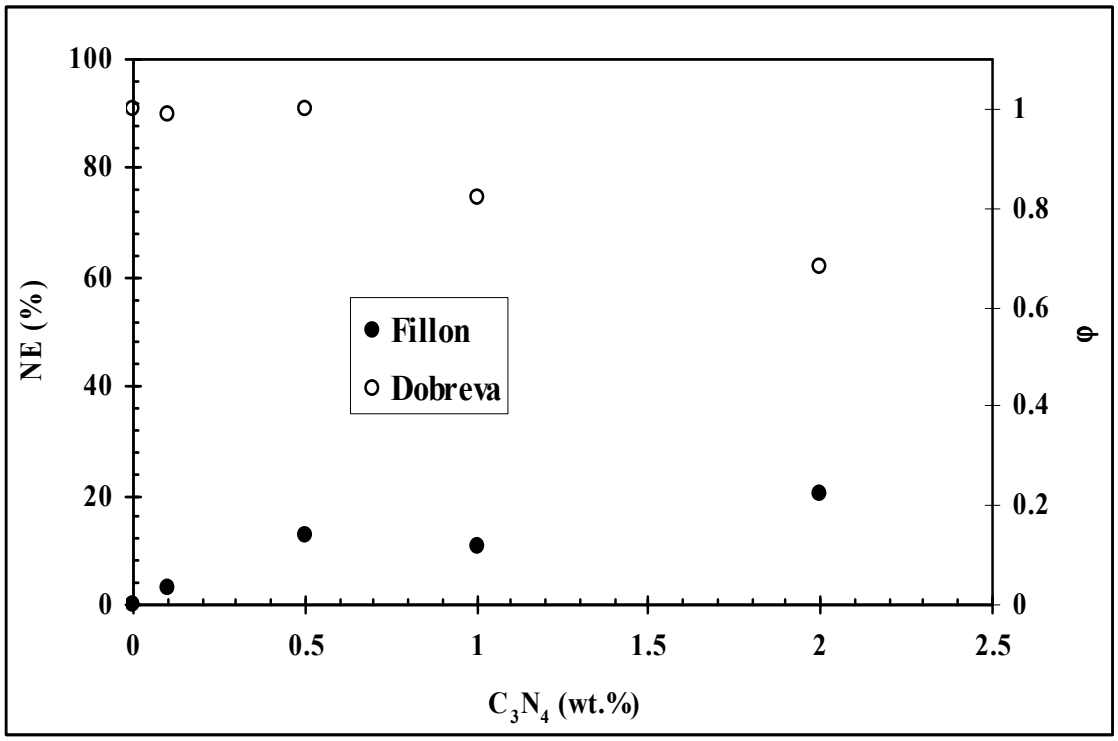
100
80
60
40
20
0
NE (%)
1
0.8
0.6
0.4
0.2
0
φ
Fillon
Dobreva
0
0.5
1
1.5
2
2.5
C3N4 (wt.%)

FIGURE 7.

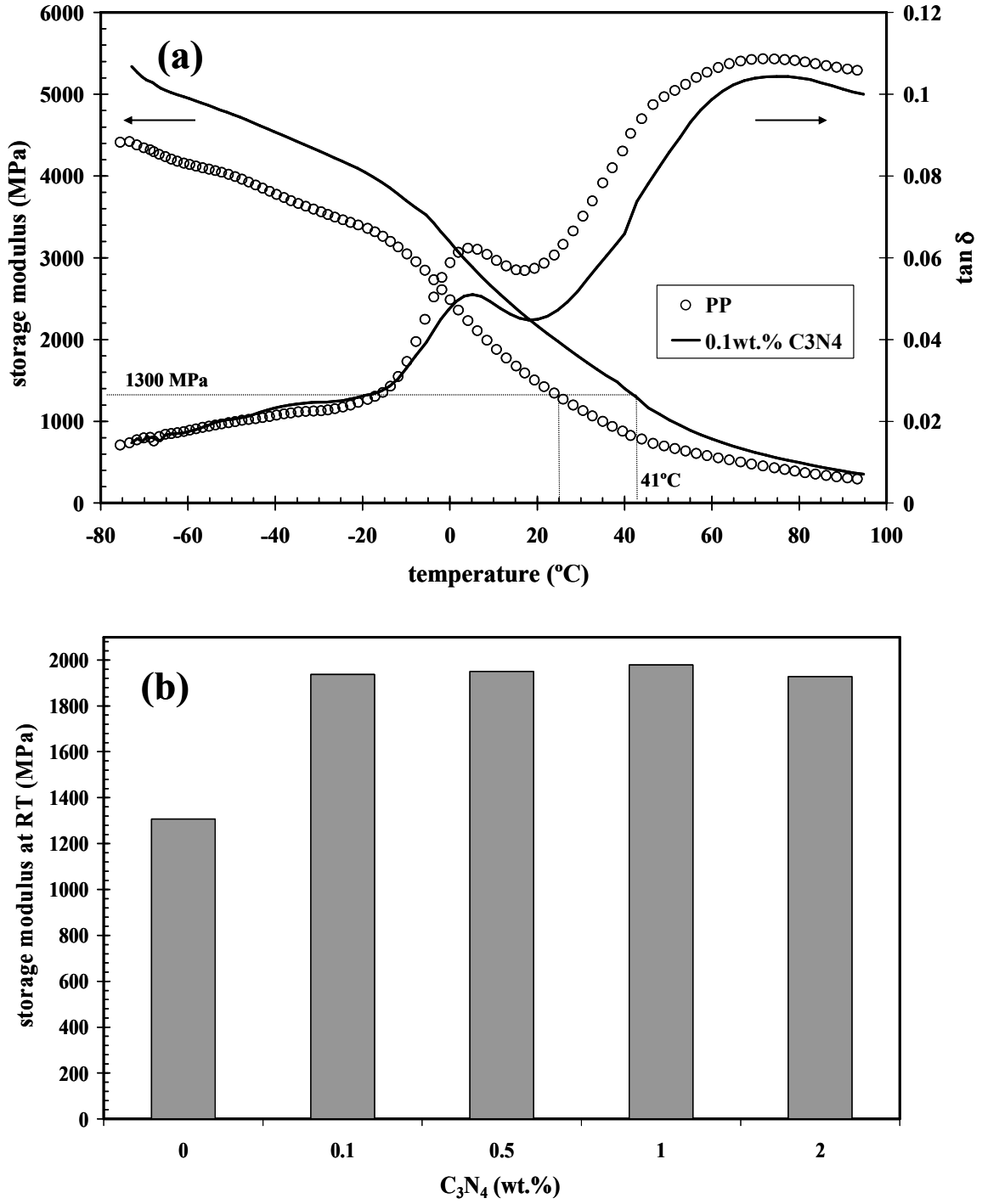
(a)
storage modulus (MPa)
tan δ
temperature (°C)
PP
0.1wt.% C3N4
1300 MPa
41°C
(b)
storage modulus at RT (MPa)
C3N4 (wt.%)

FIGURE 8.